Coupling Cloud Processes with the Large-Scale Dynamics Using the Cloud-Resolving Convection Parameterization (CRCP)

WOJCIECH W. GRABOWSKI

National Center for Atmospheric Research, Boulder, Colorado*

(Manuscript received 12 April 2000, in final form 19 September 2000)

ABSTRACT

A formal approach is presented to couple small-scale processes associated with atmospheric moist convection with the large-scale dynamics. The approach involves applying a two-dimensional cloud-resolving model in each column of a three-dimensional large-scale model. In the spirit of classical convection parameterization, which assumes scale separation between convection and the large-scale flow, the cloud-resolving models from neighboring columns interact only through the large-scale dynamics. This approach is referred to as Cloud-Resolving Convection Parameterization (CRCP). In short, CRCP involves many two-dimensional cloud-resolving models interacting in a manner consistent with the large-scale dynamics.

The approach is first applied to the idealized problem of a convective–radiative equilibrium of a two-dimensional nonrotating atmosphere in the presence of SST gradients. This simple dynamical setup allows comparison of CRCP simulations with the cloud-resolving model results. In these tests, the large-scale model has various horizontal grid spacings, from 20 to 500 km, and the CRCP domains change correspondingly. Comparison between CRCP and cloud-resolving simulations shows that the large-scale features, such as the mean temperature and moisture profiles and the large-scale flow, are reasonably well represented in CRCP simulations. However, the interaction between ascending and descending branches through the gravity wave mechanism, as well as organization of convection into mesoscale convective systems, are poorly captured. These results illustrate the limitations of not only CRCP, but also convection parameterization in general.

The CRCP approach is also applied to the idealized problem of a rotating constant-SST aquaplanet in convective–radiative equilibrium. The global CRCP simulation features pronounced large-scale organization of convection within the equatorial waveguide. A prominent solitary equatorial ''super cloud cluster'' develops toward the end of the 80-day long simulation, which bears a strong resemblance to the Madden–Julian oscillation observed in the terrestrial Tropics.

1. Introduction

Clouds and cloud-related small-scale processes play important roles in large-scale atmospheric flows and are essential for both weather and climate. At the same time, however, representing cloud processes in large-scale models is one of the most fundamental, challenging, and long-standing problems in atmospheric research. The essence of the problem stems from the range of spatial scales on which cloud processes affect large-scale and global flows. These scales cover a spectrum from a fraction of a kilometer (e.g., boundary layer processes, convective cloud dynamics), to scales of moist global flows (e.g., extratropical cyclones, convectively coupled waves in the equatorial waveguide, monsoon circulations). Resolving deep convection in an atmospheric general circulation model (AGCM) requires horizontal grid spacing of the order of 1 km (e.g., Grabowski et al. 1996; Grabowski 1998; Weisman et al. 1997), which is beyond current computational capabilities. Consequently, AGCMs and Limited Area Models (LAMs) are forced to rely on subgrid-scale modeling to represent (''parameterize'') clouds and cloud-related small-scale processes.

The increase of computational power over the last decade permitted the study of clouds (tropical deep convective clouds in particular) and their impact on radiative and surface processes on timescales relevant for the climate problem. These studies rely on numerical models that are based on nonhydrostatic dynamics and that predict formation of cloud condensate (water droplets and ice particles) as well as development and fallout of solid and liquid precipitation particles. These models are referred to as cloud-resolving models (CRMs). In studies relevant to the climate problem, CRMs are usually driven by either observed large-scale conditions

* The National Center for Atmospheric Research is sponsored by the National Science Foundation.

Corresponding author address: Dr. Wojciech W. Grabowski, NCAR, P.O. Box 3000, Boulder, CO 80307-3000
E-mail: grabow@ncar.ucar.edu

(i.e., large-scale advective tendencies for moisture and temperature, and large-scale winds) or use idealized scenarios (e.g., radiative forcing alone). The computational domains applied are large enough for an ensemble of clouds to be simulated. This approach is referred to as cloud-resolving modeling or a cumulus ensemble modeling approach, for example, Soong and Ogura (1980), Xu and Randall (1996), Grabowski et al. (1996 and references therein). In CRMs, all relevant small-scale and mesoscale processes (such as cloud dynamics and microphysics, radiative transfer, surface fluxes, convection organization, etc.) are coupled in a natural way. This is seldom the case when separate parameterizations of these processes are used within a single column of AGCMs or LAMs.

Considerable effort has been devoted in recent years to evaluate the performance of CRMs for the case of tropical deep convection using data gathered in observational campaigns such as GARP Atlantic Tropical Experiment (GATE) and Tropical Ocean Global Atmosphere Coupled Ocean–Atmosphere Response Experiment (TOGA COARE) (e.g., Xu and Randall 1996; Grabowski et al. 1996, 1998; Wu et al. 1998, 1999; Su et al. 1999; Krueger and Lazarus 1999). Among other aspects, these studies compared results obtained using 2D and 3D frameworks (e.g., Grabowski et al. 1998) and also compared CRMs to results produced by single-column models of the GCMs (Krueger and Lazarus 1999). These studies documented that 2D CRMs offer a meaningful representation of tropical deep convection, especially when compared with results from single-column models. In the conclusion of their study, Grabowski et al. (1998) state that their numerical results ''support the notion that, as long as high frequency temporal variability is not of primary importance, low resolution two-dimensional simulations can be used as realizations of tropical cloud systems in the climate problem and for improving and/or testing cloud parameterizations for large-scale models.'' Additional support for the 2D models comes from the studies of Wu et al. (1998, 1999), who applied the 2D CRM to study evolution of TOGA COARE convection during a several-week-long period, which included an active phase of a Madden–Julian oscillation (MJO, e.g., Madden and Julian 1994 and references therein) and an associated westerly wind burst. The numerical results from Wu et al. compared favorably with a variety of observations (surface, radar, satellite). Consequently, one can argue that the 2D dynamics seem sufficient to realistically mimic interactions among relevant small-scale and mesoscale processes on timescales much longer than a lifetime of a single cloud or cloud system.

The above conclusion suggests that one can design an approach in which a 2D cloud-resolving model is applied in each column of the large-scale model to represent subgrid-scale cloud processes. Grabowski and Smolarkiewicz (1999, hereafter GS99) proposed such an approach, and called it the Cloud-Resolving Convection Parameterization (CRCP). The CRCP follows a traditional strategy in convection parameterization because it assumes scale separation between convection and the large-scale dynamics. Consequently, cloud-resolving models from neighboring columns interact only through the large-scale dynamics and no cloud-scale information is directly transferred from one large-scale model column to the other. Although computationally challenging, CRCP is ideally suited for parallel computers and can operate with one to two orders of magnitude fewer computations than a 3D cloud-resolving large-scale model.

The CRCP bears some conceptual similarity to the idea of using the linear eddy model, a 1D analog of turbulent stirring and molecular diffusion (Kerstein 1988), to represent subgrid-scale processes in numerical models of engineering reactive turbulent flows. Such flows involve many decades of spatial scales separating the resolved scales (i.e., scales at which turbulent kinetic energy is generated) from the dissipation scales (the Kolmogorov and Batchelor microscales). Since these dissipative processes are essential for the volume-averaged rates of chemical reactions, an adequate representation of the microscale processes and associated chemical reactions is essential. Menon et al. (1993) applied the linear eddy model inside every gridbox of the resolved-flow model to represent subgrid-scale turbulent mixing and chemical reactions. The linear eddy model has also been applied to problems of cumulus and stratocumulus entrainment (Krueger 1993; Krueger et al. 1997) and the impact of cumulus entrainment on cloud droplet spectra (Su et al. 1998).

It can also be argued that coupling between large-scale and cloud-scale dynamics within a single dynamical framework is required if one aims to study the effects of cloud physics on the large-scale circulations and climate (see discussion in Grabowski 2000). This is particularly important for the coupling between clouds and radiative transfer. For instance, the sizes of cloud particles are an important factor in the interaction of clouds with solar radiation (e.g., Grabowski et al. 1999; Wu et al. 1999). However, sizes of cloud particles are determined by both the cloud dynamics and cloud microphysics. Consequently, realistic prediction of cloud particle sizes in AGCMs, which do not include cloud dynamics is physically limited. Another example is the coupling between cloud physics and surface processes. As shown by Grabowski et al. (1999), sizes of precipitation particles play an important role in the strength of the convective and mesoscale downdrafts and consequently in the thermodynamic regime of the tropical boundary layer. The approach advocated in this paper allows the inclusion of effects of cloud physics (cloud dynamics and cloud microphysics) into large-scale models of weather and climate.

The purpose of this paper is to discuss the CRCP approach in more detail than in GS99 and to use computational examples to illustrate the limitations of CRCP and its application to global modeling. Details of the CRCP are presented in the next section. Section 3 presents a comparison between CRCP simulations and a cloud-resolving simulation of the idealized 2D flow featuring deep convection. The comparison exposes limitations of the CRCP technique due to the scale separation assumption. Section 4 discusses application of the CRCP technique to the idealized problem of a convective–radiative equilibrium on a rotating constant sea surface temperature (SST) aquaplanet. The closing discussion is presented in section 5, and conclusions are drawn in section 6.

2. The Cloud-Resolving Convection Parameterization

The strategy underlying the CRCP approach is to consider two distinct models coupled in a particular way. The first is a 3D large-scale flow model (e.g., a LAM or a GCM). The large-scale model uses a horizontal grid length of ~100 km. The second model is a 2D cloud-scale model formulated on the x–z plane aligned E–W and embedded in each column of the large-scale model. The alignment of the cloud-scale model is motivated by the fact that vertical shear of the horizontal time-averaged flow (which is important for convection organization) tends to be predominantly in the E–W direction in terrestrial large-scale flows. This is the alignment of the 2D cloud-resolving simulations of tropical convection driven by observed large-scale conditions (e.g., Grabowski et al. 1996, 1998, 1999; Wu et al. 1998, 1999). Cloud-scale and large-scale models use the same vertical grid. The cloud-scale model applies sufficiently small horizontal grid length to resolve moist convective dynamics (~1 km). The cloud-scale model is periodic in the horizontal, an assumption important for energy and water conservation [see Grabowski et al. (1996) for a discussion].

The large-scale model employs inviscid moist equations. The model variables are the three components of velocity, the potential temperature, and the mixing ratios for water vapor, cloud condensate, and precipitation. The anelastic system of equations can be compactly written as

$$\frac{\mathcal{D}\mathbf{U}}{\mathcal{D}t} = -\boldsymbol{\nabla}\Pi + \mathbf{k}gB + \mathbf{i}F_{\mathrm{CS}}^{U} + D_{\mathbf{U}} \quad (1a)$$

$$\boldsymbol{\nabla}\cdot(\rho_o\mathbf{U}) = 0 \quad (1b)$$

$$\frac{\mathcal{D}\Theta}{\mathcal{D}t} = F_{\mathrm{CS}}^{\Theta} + D_{\Theta} \quad (1c)$$

$$\frac{\mathcal{D}Q_v}{\mathcal{D}t} = F_{\mathrm{CS}}^{Q_v} + D_{Q_v} \quad (1d)$$

$$\frac{\mathcal{D}Q_c}{\mathcal{D}t} = F_{\mathrm{CS}}^{Q_c} + D_{Q_c} \quad (1e)$$

$$\frac{\mathcal{D}Q_p}{\mathcal{D}t} = F_{\mathrm{CS}}^{Q_p} + D_{Q_p}. \quad (1f)$$

Here, $\mathbf{U} = (U, V, W)$ is the large-scale flow in the E–W, N–S, and vertical direction, respectively; Θ is the potential temperature, and Q_v, Q_c, and Q_p are mixing ratios for water vapor, cloud condensate (i.e., condensed water carried by the flow), and precipitation (condensed water that falls relative to the air). Here $\mathcal{D}/\mathcal{D}t \equiv \partial/\partial t + \mathbf{U}\cdot\boldsymbol{\nabla}$; Π is the pressure perturbation with respect to a geostrophically balanced ambient state, normalized by the anelastic reference density ρ_o; $\mathbf{i}$ and $\mathbf{k}$ are unit vectors in the E–W and vertical directions, respectively; the buoyancy $B = (\Theta - \Theta_e)/\Theta_o + \epsilon(Q_v - Q_{v_e}) - Q_c - Q_p$, where Θ_e and Q_{v_e} are ambient potential temperature and water vapor profiles, Θ_o is the reference potential temperature profile, $\epsilon = R_v/R_d - 1 \approx 0.607$; and g is the gravitational acceleration. The D terms are forcings that are not directly represented in (1), such as the Coriolis acceleration, metric terms for the spherical system, and optional gravity wave absorbers in the thermodynamic equations. The F_{CS} terms on the right-hand side of (1a)–(1f) represent the cloud-scale model feedback. The large-scale model does not include explicit representations of small-scale processes such as surface fluxes, radiative transfer, phase changes, latent heating, or precipitation fallout. These are included in the cloud-scale model equations (2) and their *effects* are transfered to the large-scale model via F_{CS} terms [for a discussion see section 2 in Grabowski et al. (1996)].

The anelastic equations of the cloud-scale model are as follows:

$$\frac{d\mathbf{u}}{dt} = -\boldsymbol{\nabla}'\pi + \mathbf{k}gb + \mathbf{i}(s_u + f_{\mathrm{LS}}^{u}) + d_{\mathbf{u}} \quad (2a)$$

$$\boldsymbol{\nabla}'\cdot(\rho_o\mathbf{u}) = 0 \quad (2b)$$

$$\frac{d\theta}{dt} = \frac{\theta_e}{T_e}\left[\frac{L_v}{c_p}(\mathrm{CON} + \mathrm{DEP}) + r\right] + s_\theta + f_{\mathrm{LS}}^{\theta} + d_\theta \quad (2c)$$

$$\frac{dq_v}{dt} = -\mathrm{CON} - \mathrm{DEP} + s_{q_v} + f_{\mathrm{LS}}^{q_v} + d_{q_v} \quad (2d)$$

$$\frac{dq_c}{dt} = \mathrm{CON} - \mathrm{ACC} - \mathrm{AUT} + f_{\mathrm{LS}}^{q_c} + d_{q_c} \quad (2e)$$

$$\frac{dq_p}{dt} = \frac{1}{\rho_o}\frac{\partial}{\partial z}(\rho_o v_t q_p) + \mathrm{ACC} + \mathrm{AUT} + \mathrm{DEP} + f_{\mathrm{LS}}^{q_p} + d_{q_p}, \quad (2f)$$

where the lowercase symbols have the same meaning as the respective uppercase symbols in (1). For example, $\mathbf{u} = (u, w)$ is the cloud-scale flow in the E–W and vertical direction, respectively; $d/dt \equiv \partial/\partial t + \mathbf{u}\cdot\boldsymbol{\nabla}'$ with $\boldsymbol{\nabla}' \equiv (\partial/\partial x, \partial/\partial z)$; etc. The s terms denote sinks/sources of E–W momentum, temperature, and moisture associated with surface processes. The f_{LS} terms represent the large-scale forcing for the cloud-scale model; L_v and

c_p are the latent heat of condensation and the specific heat at constant pressure; and θ_e and T_e are the environmental potential temperature and temperature profiles (the same as the environmental profiles of the large-scale model at a given large-scale model column). The sources on the right-hand-side of (2c)–(2f) describe the formation of cloud condensate from water vapor (CON), autoconversion of cloud condensate into precipitation (AUT), accretion of cloud condensate by precipitation (ACC), and source/sink of precipitation due to deposition/evaporation of water vapor on/from precipitation particles (DEP). These sources are represented using the simple scheme of Grabowski (1998, hereafter G98). The temperature tendency due to radiative flux divergence in (2c) is r and v_t in (2f) is the sedimentation velocity of the precipitation water q_p. The d terms appearing in the prognostic equations symbolize viscous forces due to the subgrid-scale turbulence (optional) and gravity wave absorbers.

The coupling formalism of the large-scale and cloud-scale models follows the strategy discussed in section 2 of Grabowski et al. (1996) for the case of a cloud-resolving model driven by observed large-scale conditions. Insofar as the kinematics is concerned, the large-scale flow (vertical shear in particular) organizes convection while the cloud-scale flow exerts a drag on the large-scale flow. Consequently, the cloud-scale and large-scale E–W flows are simply coupled by relaxing to each other on a finite timescale:

$$F^U_{\rm CS} = -\frac{U - \langle u \rangle}{\tau_m} \tag{3a}$$

$$f^u_{\rm LS} = -\frac{\langle u \rangle - U}{\tau_m}, \tag{3b}$$

where τ_m is the timescale of the kinematic coupling (taken as $\tau_m = 1$ h in experiments reported in this paper), and the $\langle \cdot \rangle$ denotes the horizontal averaging of a cloud-scale dependent variable, for example,

$$\langle u(x, z, t)|_{(X,Y)} \rangle \equiv \frac{1}{L} \int_{-L/2}^{L/2} u(\xi, z, t)|_{(X,Y)}\, d\xi, \tag{4}$$

where L is the extent of the horizontal domain used in each cloud-scale model.

Because convective heating and moistening are essential for the large-scale dynamics, all thermodynamic fields are coupled instantaneously (i.e., through numerically consistent averaging procedures). The coupling follows a traditional approach to convection parameterization in which large-scale dynamics provides the so-called large-scale forcing for convection, and convection feeds back the so-called convective response (e.g., section 2 in Grabowski et al. 1996). Decomposing the model variables into the large-scale and cloud-scale components, and employing the scale separation arguments, leads to the representation of the large-scale forcing terms for thermodynamics variables $f_{\rm LS}$ in the cloud-scale model equations (2) in terms of the advective tendencies and forces from the large-scale model:

$$f^\theta_{\rm LS} = -\mathbf{U} \cdot \nabla \Theta + D_\Theta \tag{5}$$

(and similar expressions for moisture variables); see section 2 in Grabowski et al. (1996) for a discussion.

The large-scale forcing terms for the E–W momentum, temperature, and moisture are applied homogeneously across the 2D cloud-scale model at a given level. However, the large-scale forcing terms for cloud condensate and precipitation are added only to the grid boxes that already have some condensate or precipitation to prevent instantaneous evaporation of typically small amounts of cloud condensate and/or precipitation, which are produced by the positive large-scale tendencies over a single time step, and to avoid negative values of these fields in the case of negative large-scale tendencies. If grid boxes at a given level are void of cloud condensate and precipitation entirely, the large-scale forcing is deposited in a small subset (consisting of four grid boxes in the examples presented below) of the cloud-scale model domain at this level. The location of the subset is selected randomly.

The $F_{\rm CS}$ terms for thermodynamic fields in the large-scale model equations (1) are implicit because the large-scale thermodynamic fields are derived from horizontal averaging of cloud-scale variables after cloud-resolving model completes its calculations, for example,

$$\Theta(X, Y, Z, t) = \langle \theta(x, z, t)|_{(X,Y)} \rangle, \tag{6}$$

where $Z \equiv z$.

The above-outlined model coupling assures that, at any given level, the thermodynamic fields of the large-scale column exactly match the horizontal average of the cloud-scale fields. However, the E–W flows match only approximately with relatively small discrepancies as illustrated a posteriori by the results presented in GS99.

The time stepping of the entire system (1)–(2) proceeds in three distinct steps.

- *Step 1.* The advective tendencies for momenta and thermodynamic variables in the large-scale model are derived. The tendencies for thermodynamic fields are added to the large-scale model forces D and they together form the large-scale forcing terms (5) for the cloud-scale model. The E–W momentum forcing (3b) is calculated as well.
- *Step 2.* The evolution of the 2D cloud field, in response to the large-scale forcing and to forcings associated with the radiative and surface processes, is calculated in parallel using the cloud-scale model inside each column of the large-scale model. As a result, new time-level thermodynamic fields are obtained for each cloud-scale model. Usually, a smaller time step (δt) has to be used in the cloud-scale models than in the large-scale model (Δt). Thus, the cloud-scale models perform several δt time steps, in order to reach

the time level $t + \Delta t$ to which the large-scale model will be updated after completing the step 3 below.

- *Step 3.* The large-scale thermodynamic fields are updated according to (6) by horizontal averaging of the cloud-scale fields for each column of the large-scale model. Updated large-scale buoyancy is applied to the vertical momentum equation (1c) of the large-scale model, and the E–W momentum forcing for the large-scale model (3a) is applied to the U-equation (1a). Derivation of the large-scale pressure gradient and its application to the large-scale momenta completes the time step Δt of the entire system.

Both the large-scale and cloud-scale models employ the nonoscillatory forward-in-time approach of Smolarkiewicz and Margolin (1997), built on the transport algorithm MPDATA reviewed recently in Smolarkiewicz and Margolin (1998). The elliptic pressure equation, which derives from the anelastic ''incompressibility'' constraint imposed on the discretized momentum equation is solved using the generalized-conjugate-residual method of Eisenstat et al. (1983), see Smolarkiewicz and Margolin (1994). The Cartesian large-scale model applied in the next section is the Eulerian variant of the two-time-level, nonhydrostatic anelastic fluid model EULAG of Smolarkiewicz and Margolin (1997). The global large-scale model applied in section 4 is that of Smolarkiewicz et al. (2001). The free-slip impermeable upper and lower boundaries are common in large-scale and cloud-scale models. Weak gravity wave absorbers are employed in the upper portion of both models to minimize wave reflection from the rigid boundary and to mimic an infinite vertical extent of the fluid. No turbulence or subgrid-scale transport parameterizations are applied in the cloud-scale model (see Margolin et al. 1999).

In summary, the modeling strategy outlined above represents many 2D cloud-resolving models coupled with each other according to the large-scale dynamics. The next two sections illustrate application of this technique to idealized problems of large-scale atmospheric dynamics.

3. Two-dimensional convective–radiative equilibrium in the presence of large-scale SST gradients

In this section, we discuss numerical simulations of a 2D convective–radiative equilibrium in the presence of large-scale SST gradients. This problem has been discussed in Raymond (1994) using parameterized convection and in Grabowski et al. (2000, hereafter GYM00) using a cloud-resolving modeling approach (see also section 5 in G98). It is anticipated that CRCP should work best when the large-scale flow is strictly two-dimensional because the orientation of the 2D cloud models (i.e., E–W vs N–S) is not an issue in such a case. However, the fact that cloud-scale models from the neighboring columns of the large-scale model interact only through the large-scale dynamics means that CRCP (and convection parameterization in general) are limited as far as propagation of small-scale and mesoscale features (such as gravity waves, cold pools, cloud systems) are concerned, as illustrated in this section.

The simulations consider 2D nonrotating flow in a periodic 4000-km-long domain. The large-scale flow is driven by an SST varying as the cosine function with 28°C in the center of the domain and 24°C at the lateral boundaries. The atmosphere is initially at rest. A prescribed horizontally homogeneous potential temperature tendency profile mimics a net radiative cooling of 1.5 K day^{-1} at all levels, that is, as in G98 and in the simulation PR in GYM00. The prescribed radiative cooling is balanced by the surface heat fluxes once the quasi-equilibrium is reached (after about a month of model time, cf. Fig. 14 in G98, Fig. 1 in GYM00). The surface fluxes are calculated using simple bulk formulas (i.e., as G98; PR in GYM00 applied a more sophisticated formulation of surface fluxes). The cloud-resolving model and the CRCP model were integrated for 60 days and results are compared for the last 20 days.

The cloud-resolving simulation was performed using a grid of about 1.8 km in the horizontal direction and a ⅓-km grid in the vertical. The time step was 15 s. A gravity wave absorber was applied in the uppermost 8 km of the 25-km-deep domain.

Several CRCP simulations were performed applying different horizontal resolutions of the large-scale model and horizontal extent of the CRCP domains. Such a strategy illustrates the fundamental assumption of scale separation inherent in CRCP and in any other convection parameterization scheme. In one of the simulations, referred to as P500, the large-scale model applied a horizontal grid length of 500 km (i.e., the large-scale model featured just eight columns) and CRCP horizontal domains were 500 km long. In a simulation at the other end of possible choices, the large-scale model applied a horizontal grid of 20 km (i.e., the large-scale model had 200 columns), and CRCP horizontal domains were just 20 km long; this simulation is referred to as P20. A few simulations between these two extremes were also performed, such as P100 and P50, that is, with a large-scale model grid (and CRCP horizontal domains) of 100 km and 50 km, respectively. The P500 simulation represents a situation typical in present-day climate models that use a horizontal resolution of a few degrees. Computational domains of a similar size were applied in cloud-resolving model simulations of tropical convection driven by observed large-scale conditions. The P20, on the other hand, represents the situation typical for weather prediction mesoscale models (e.g., LAMs) that apply a horizontal grid of a few tens of kilometers. In this case, CRCP plays the role of a convection parameterization as used in a mesoscale model, for example, a Kain–Fritsch scheme as applied in Liu et al. (2001).

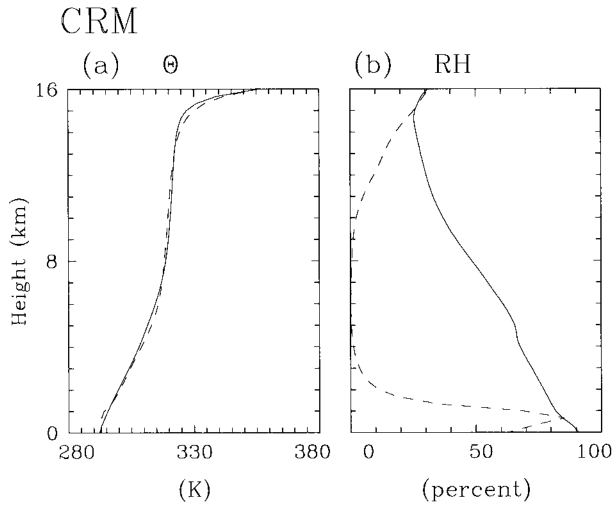

FIG. 1. Profiles of (a) the potential temperature and (b) the relative humidity for the ascending branch (solid lines) and the descending branch (dashed lines) of the large-scale circulation for the cloud-resolving simulations.

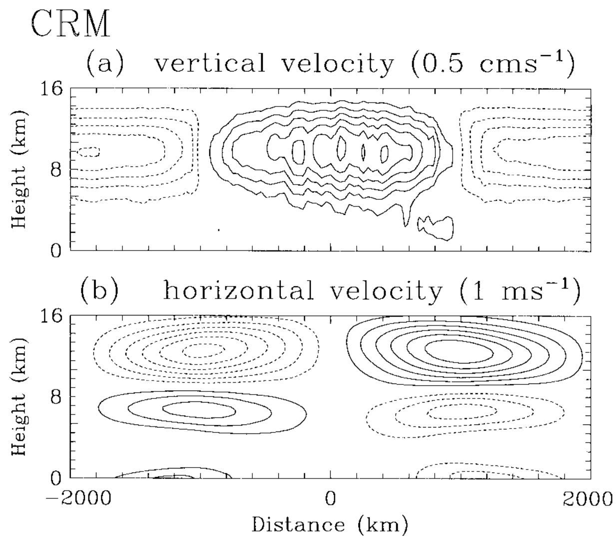

FIG. 2. Spatial distribution of (a) the vertical velocity and (b) the horizontal velocity for the cloud-resolving simulation. The time average is made over the period of day 40 to day 60 and a moving average is applied over the 400-km horizontal distance to smooth the fields. Contour intervals are (a) 0.5 cm s^{-1} and (b) 1 m s^{-1}. Positive (negative) contours are shown by solid (dashed) lines and the zero contour is not shown.

All the CRCP simulations apply identical setups in terms of the prescribed radiative cooling and the surface flux algorithm inside the CRCP computational domains. The vertical grid spacing is larger than in the cloud-resolving simulation (½ rather than ⅓ km). The cloud-scale models embedded in all columns of the large-scale model apply a horizontal grid of 1 km and feature gravity wave absorbers in the uppermost 8 km of the 25-km-deep domain. The SST in each CRCP model is assumed constant and is defined as the SST at the center of the large-scale model column. The surface fluxes are calculated inside cloud-scale models using the local temperature, moisture, and wind fields. The large-scale model time step is 60 s, whereas cloud-scale models are integrated with a 15-s time step.

All simulations feature the quasi-equilibrium large-scale flow with an ascending branch and deep convection over warm SSTs, and a dry cloud-free descending branch over cold SSTs (cf. GYM00). Figures 1–4 show selected results from the cloud-resolving simulation. Figure 1 shows the potential temperature and the relative humidity profiles averaged over the last 20 days and over a 500-km horizontal distance near the center of the domain and near the lateral periodic boundaries. These profiles are referred to as profiles inside ascending and descending branches, respectively. Figure 2 shows the time-averaged large-scale horizontal and vertical velocities. Figure 3 shows evolution of the large-scale horizontal velocity profiles averaged over a 500-km distance near the maximum SST gradients (i.e., at $x = -1000$ km for the left cell and $x = 1000$ km for the right cell). Finally, Fig. 4 shows the Hovmöller (time–space) diagram of the surface precipitation for the last 20 days of the simulation.

Figures 5 to 8 show corresponding results from the CRCP simulations P500 and P20 (Fig. 8 also shows data for P50). The CRCP simulations appear to capture the large-scale features reasonably well. The P500 simulation predicts a considerably warmer upper troposphere compared to P20 and to the cloud-resolving simulation (Figs. 1 and 5). It also fails to represent the extreme dryness of the descending branch. This is probably due to the low spatial resolution of the large-scale

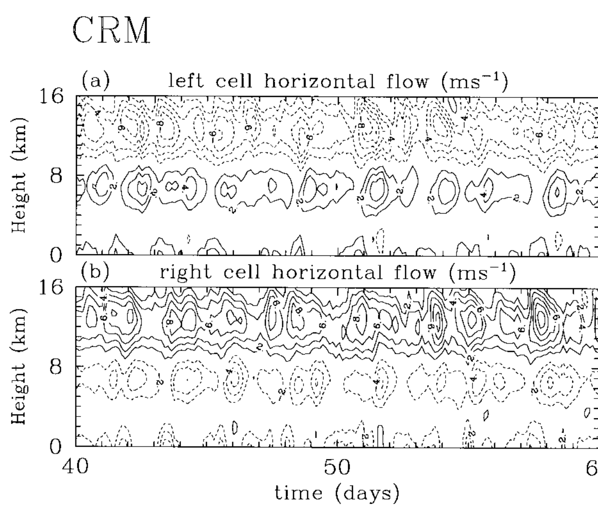

FIG. 3. Evolution of the horizontal wind profiles averaged in space as explained in text for the last 20 days of the cloud-resolving simulation. The profiles for the (a) left-hand half and (b) right-hand half of the domain. Contour interval is 2 m s^{-1}. Positive (negative) contours are shown by solid (dashed) lines and the zero contour is not shown.

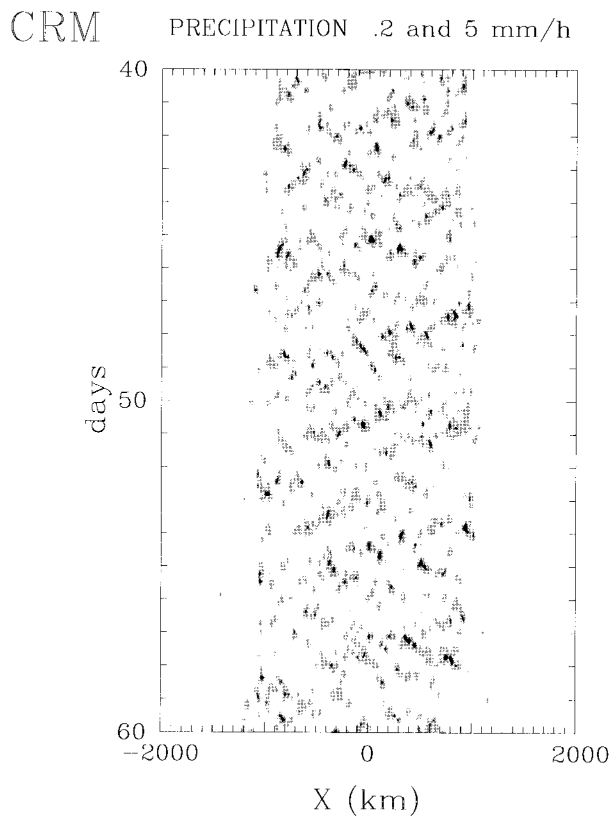

FIG. 4. Hovmöller diagram of the surface precipitation rate for the last 20 days of the cloud-resolving simulation. Precipitation intensity larger than 0.2 and 5 mm h^{-1} is shown using light and dark shading, respectively.

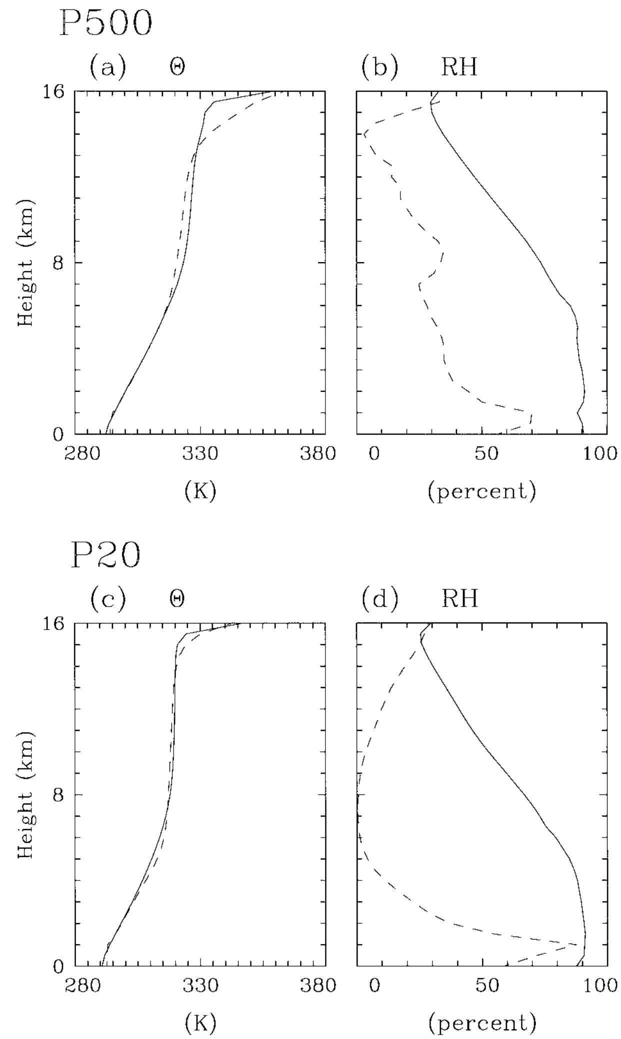

FIG. 5. As in Fig. 1 but for the CRCP simulations (a) and (b) P500 and (c) and (d) P20.

model, which features just eight columns in P500. The P20 simulation, on the other hand, is slightly less stable in the upper troposphere, which affects the strength of the large-scale upper-tropospheric circulation (cf. Figs. 6c and 6d). As discussed in GYM00, the large-scale descent over cold SSTs is the primary mechanism for balancing the (prescribed) radiative cooling. Weaker stability in the upper troposphere requires stronger large-scale descent and consequently stronger large-scale circulation. Both P500 and P20 overpredict the mean relative humidity in the ascending branch (Figs. 5b and 5d) compared to the cloud-resolving simulation (Fig. 1b). The relative humidity is higher by 10%–15% for P20 and by 15%–20% for P500 throughout the most of the troposphere near the center of the domain.

The large-scale flows in the cloud-resolving and CRCP simulations are compared in Figs. 2, 3, 6, and 7. In general, the time- and space-averaged flows (Figs. 2 and 6) are similar. They all feature upper-tropospheric outflow from the ascending branch with deep convection, and inflows at the surface and in the middle troposphere. Some caution is due, however, when comparing large-scale flows from cloud-resolving and CRCP simulations. For instance, the cloud-resolving results and P20 results were smoothed in the horizontal direction (over 400 km for Fig. 2 and Figs. 6c and 6d) to obtain mean flows with cloud-scale and mesoscale motions filtered out. The P500 results, on the other hand, represent time-averaged large-scale flow from eight columns of the outer model and Figs. 6a and 6b are affected by linear interpolation performed during plotting.

Evolution of the horizontal flow near the maximum SST gradients (Figs. 3 and 7) are different for cloud-resolving and CRCP simulations. Cloud-resolving results show horizontal wind fluctuations associated with the quasi-two-day oscillations. As discussed in section 5 of GYM00, these oscillations result from the coupling between convection and gravity waves (or bores; Mapes 1993; Mapes 1998). These waves are launched from the ascending branch and propagate into the descending branch. The interplay between convection and gravity wave dynamics within the 2D periodic computational domain results in the quasi-two-day oscillations in the strength of convection and the large-scale flow. The

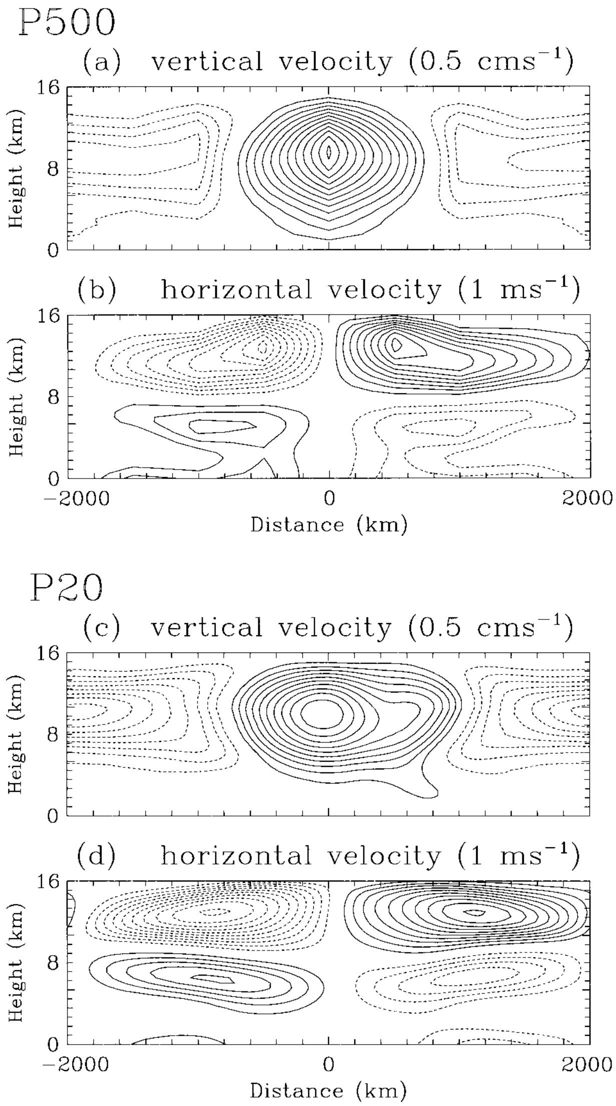

FIG. 6. As in Fig. 2 but for the CRCP simulations (a) and (b) P500 and (c) and (d) P20.

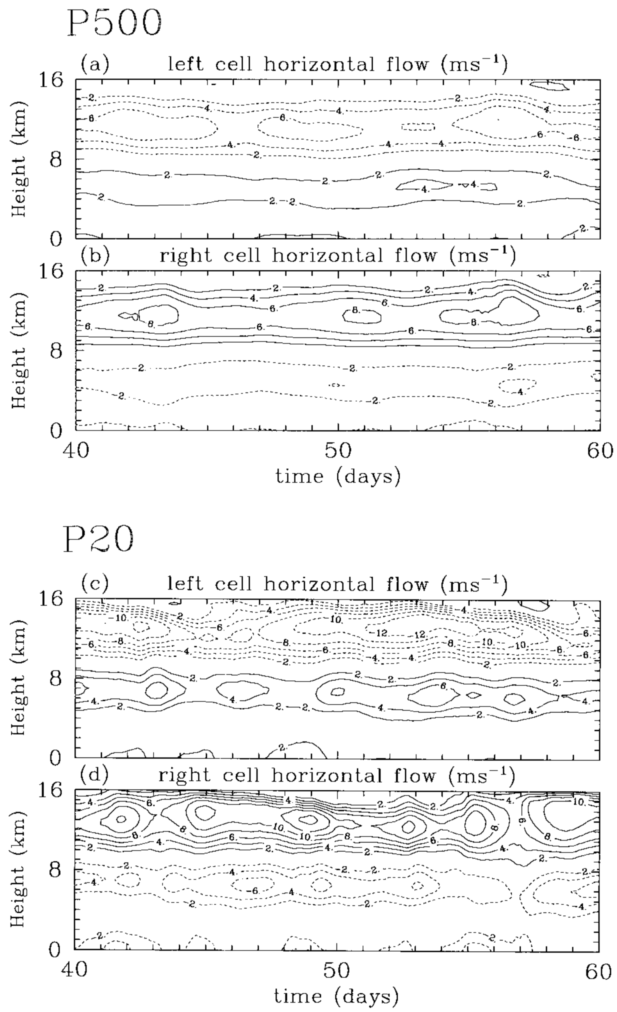

FIG. 7. As in Fig. 3 but for the CRCP simulations (a) and (b) P500 and (c) and (d) P20.

gravity wave response is quantified in GYM00 using normal mode analysis. Neither P20 nor P500 (Fig. 7) shows such a variability of the large-scale flow. However, the P20 features stronger temporal variability than P500 as one might expect.

As far as convection organization is concerned, the key differences are illustrated in Hovmöller diagrams of the surface precipitation (Figs. 4 and 8). In the cloud-resolving simulation (Fig. 4), the convection is organized into mesoscale convective systems with a horizontal extent between 100 and 300 km. These systems travel across the central part of the domain with typical speeds of about 10 m s^{-1} (see also Fig. 13 in G98 and Fig. 3a in GYM00). Latent heating associated with these systems is responsible for the generation of gravity waves mentioned above (see also Oouchi 1999).

Convection organization in the CRCP simulations is illustrated in Fig. 8. The P500 features organized convection only in the central 500-km column of the large-scale model. Convective systems propagate across the periodic domain either from left to right (e.g., day 44 or 58) or from right to left (e.g., day 53) with speeds similar to those in the cloud-resolving simulation. Apparently, the CRCP domains in P500 are large enough to capture the convective and mesoscale dynamics responsible for convection organization. However, the convective systems are trapped inside the periodic CRCP domain over the highest SST and are unable to propagate into adjacent columns of the large-scale model. The horizontal extent of the systems appears smaller than in the cloud-resolving case. Convection in other large-scale model columns is much weaker and unorganized.

As the horizontal gridlength of the large-scale model and extent of CRCP domains decrease, the pattern of surface precipitation changes dramatically. The P100 (not shown) and P50 simulations (Fig. 8b) feature scat-

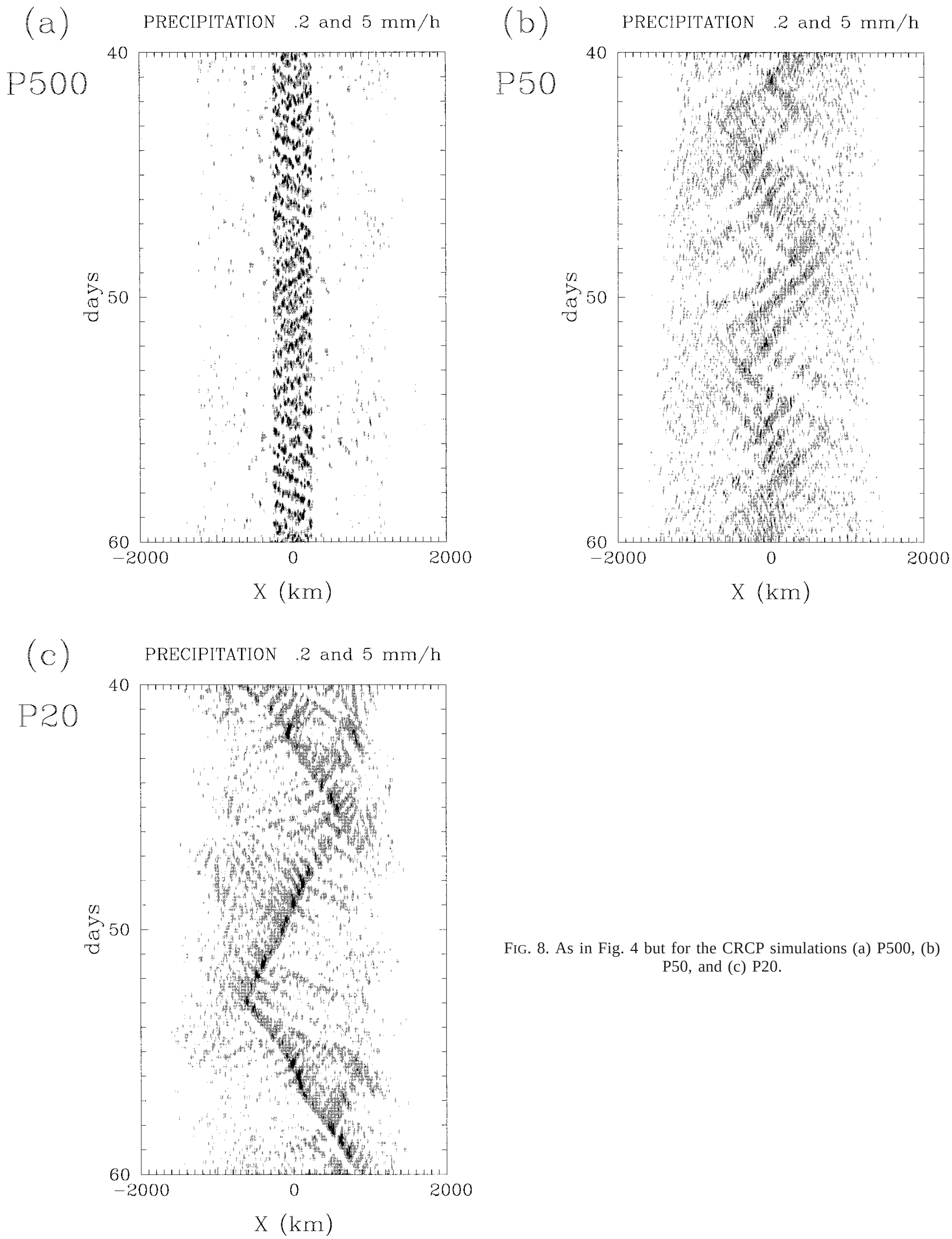

FIG. 8. As in Fig. 4 but for the CRCP simulations (a) P500, (b) P50, and (c) P20.

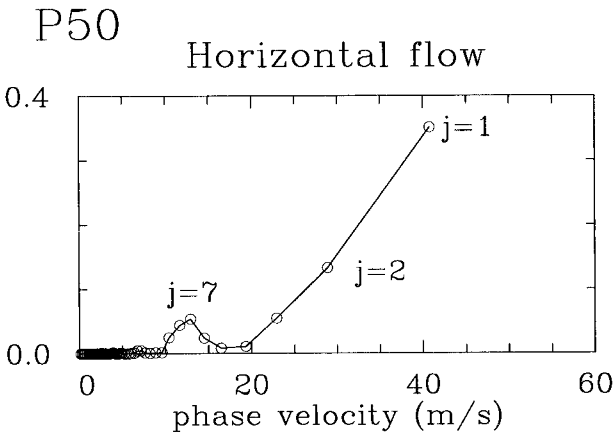

FIG. 9. Spectra (i.e., the square of the expansion coefficients) for the horizontal winds as a function of the normal mode phase speed for the P50 simulation. The modes corresponding to $j = 1$, $j = 2$, and $j = 7$ are marked.

tered convection grouped into bands that propagate from one end of the warm SSTs to the other and back with a timescale of 8–10 days. These bands merge into a single line of enhanced convection in P20 (Fig. 8c). The line travels slowly across the warm SSTs. Individual clouds or small cloud systems propagate toward the line, merge with it, and often continue to travel away from the line. These clouds or systems move with speeds comparable to systems in the cloud-resolving and P500 simulations (Figs. 4 and 8a).

The differences in the interaction between convection and the large-scale flow in the cloud-resolving and CRCP simulations were further investigated using normal mode analysis as in GYM00. Results for P50 are shown in Figs. 9 and 10. The figures show normal model decomposition of the mean large-scale horizontal flow and the Hovmöller diagrams of the decomposition coefficients for the evolving large-scale horizontal flow corresponding to $j = 1$, $j = 2$, and $j = 7$ baroclinic modes. These three modes have shapes that are traditionally referred to as the first, the second, and the third tropospheric baroclinic mode, respectively (see section 4 in GYM00). Figures 9 and 10 should be compared to Figs. 13a and 17 in GYM00, which show results for the cloud-resolving simulation. The mean circulation (Fig. 9) is dominated by $j = 1$ and $j = 2$ modes; the $j = 7$ mode has a considerably smaller amplitude in the CRCP simulation than in its cloud-resolving counterpart. The most important difference, however, is associated with the propagation of various modes as shown in Fig. 10. Contrary to results from the cloud-resolving simulation (Fig. 17 in GYM00), analysis of the P50 large-scale horizontal flow shows mode propagation in the physical domain with speeds much slower than the theoretical speed of a given mode. For instance, perturbations associated with $j = 1$ and $j = 2$ modes (Figs. 10a and 10b) tend to propagate across the domain with very similar speeds (between 10 and 15 m s^{-1}), whereas their theoretical phase velocities, according to Fig. 9, are about 40 and 30 m s^{-1}, respectively. These results show that the CRCP simulation is unable to represent the coupling between convection and wave dynamics as simulated by the cloud-resolving model.

In summary, all CRCP simulations predict similar large-scale flow in radiative–convective equilibrium. The organization of convection, and the interaction between ascending and descending branches through the gravity wave mechanism, on the other hand, differ considerably among all the simulations. These results illustrate the limitations of not only CRCP, but convection parameterization in general.

4. Convective–radiative equilibrium on a rotating constant-SST aquaplanet

To illustrate the interactions between large-scale and cloud-scale dynamics in the context of global-scale flows, we consider an idealized problem of convective–radiative equilibrium on a rotating constant-SST aquaplanet with the size and rate of rotation the same as the earth. A similar problem was considered by Sumi (1992), who applied a traditional convection parameterization approach.

The global model is the anelastic nonhydrostatic two-time-level nonoscillatory forward-in-time Eulerian/semi-Lagrangian Navier–Stokes solver in spherical geometry (Smolarkiewicz et al. 2001). The global model has low resolution in the E–W and N–S directions (32 $\times$ 16) and uses 51 levels in the vertical with a uniform grid length of 0.5 km. The global model time step is 12 min.

The 2D cloud-scale models in each column of the global model have horizontal periodic domains of 200 km with a 2-km grid length. We take advantage of the fact that the horizontal domain of CRCP periodic models inside each column of the global model can be selected arbitrarily. The choice herein represents a compromise between the computational cost (which increases almost linearly with the number of columns in the CRCP model domain) and the horizontal extent of the domain used in cloud-resolving simulations of tropical convection driven by observed large-scale conditions (typically in the range of 500–1000 km). The vertical grid is the same as in the global model. The model time step is 30 s. In addition, the gravity wave absorber is used in the uppermost 9 km of each cloud model with an inverse of the characteristic timescale increasing linearly from zero at the bottom of the absorber to 1/600 s^{-1} at the top of each model domain.

The globally uniform SST is assumed at 30°C (303.16 K) and the effects of radiative processes on the atmosphere are prescribed by applying a constant-in-time cooling rate profile. The cooling rate is 1.5 K day^{-1} below 12 km, linearly decreases from 1.5 K day^{-1} to zero between 12 and 15 km, and is zero above 15 km. The sounding used to prescribe initial thermodynamic

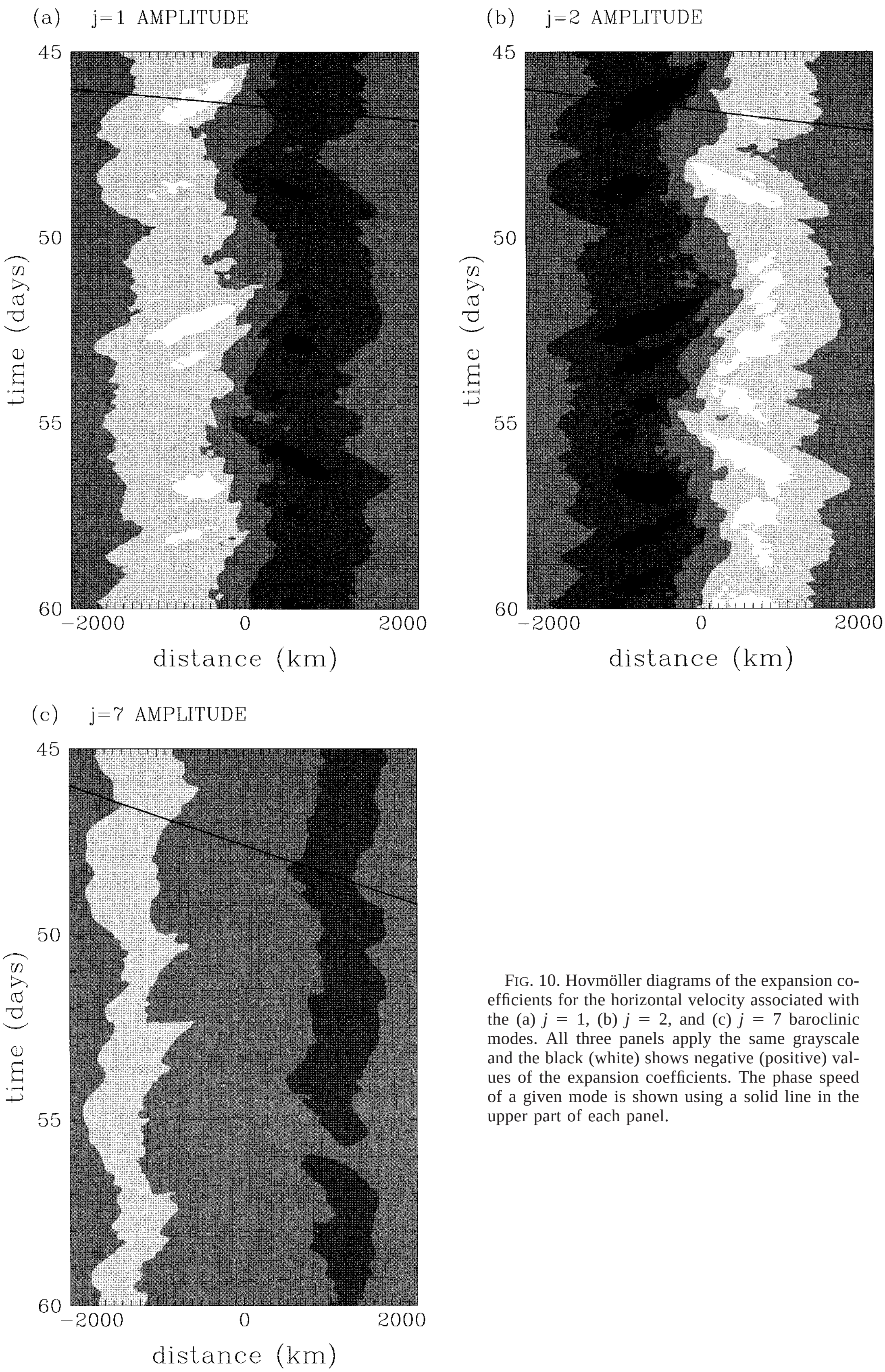

FIG. 10. Hovmöller diagrams of the expansion coefficients for the horizontal velocity associated with the (a) $j = 1$, (b) $j = 2$, and (c) $j = 7$ baroclinic modes. All three panels apply the same grayscale and the black (white) shows negative (positive) values of the expansion coefficients. The phase speed of a given mode is shown using a solid line in the upper part of each panel.

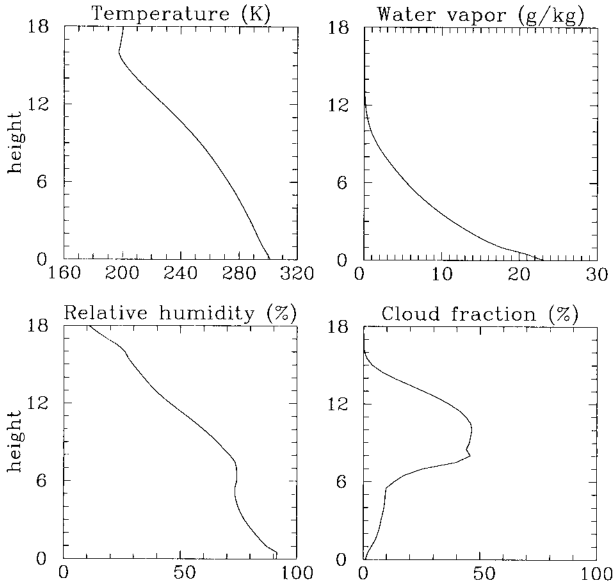

Fig. 11. Profiles of the globally and temporally averaged temperature, water vapor mixing ratio, relative humidity, and cloud fraction for the CRCP simulation of the rotating constant-SST aquaplanet.

profiles as well as model reference and environmental profiles is taken from the 0000 GMT 1 September 1974 GATE sounding (i.e., as in Grabowski et al. 1996, 1998, 1999). The global atmosphere is assumed to be initially at rest. Note that simulations reported in Sumi (1992) were initialized from globally averaged fields of the terrestrial large-scale flow.

The global CRCP model is initialized in the following manner. First, a single 2D cloud model, the same as applied in all columns of the global model, is run into convective–radiative equilibrium assuming the SST and radiative cooling profile as described above, and no mean flow. A relaxation term with a timescale of 12 h is added to the horizontal momentum equation for the single model simulation to maintain the vanishing mean flow. Without such control, 2D simulations tend to excite oscillatory patterns in the mean flow, presumably due to exaggerated wave–mean flow interactions in two spatial dimensions (cf. Held et al. 1993). The single model is integrated for a period of 60 days, which is sufficient to establish the radiative–convective equilibrium. Snapshots of the model-generated cloud-scale fields at day 60 (i.e., the velocities, potential temperature, and water variables) are distributed to all columns of the global model. The temperature in all 2D cloud-scale models is randomly perturbed with the amplitude of 0.3 K. The cloud-scale model thermodynamic fields are then averaged into the global model grid. An atmosphere at rest is initially assumed in the global model (i.e., $U = W = 0$). The entire system is then integrated for 80 days.

Figure 11 shows globally averaged profiles of the thermodynamic fields from the last 20 days of the simulation. The panels show profiles of the temperature, water vapor mixing ratio, relative humidity, and the cloud fraction. The cloud fraction is defined as a fraction of cloud-scale model grid boxes at a given level with a condensate mixing ratio, including both cloud and precipitation, larger than 0.1 g kg^{-1}. The globally averaged profiles do not evolve significantly and those shown in the figure are similar to the single cloud-resolving model profiles used to initialize the global CRCP model. The characteristic features include: weaker stability of the upper troposphere compared to the lower troposphere, decrease of the relative humidity with height, and a higher fraction of middle- and upper-tropospheric ice clouds as compared to water clouds in the lower troposphere. The air temperature and water vapor mixing ratio at the surface are about 1.5 K and 5 g kg^{-1} lower than the assumed values of the sea surface. The globally averaged precipitable water associated with the moisture profile shown in Fig. 7b is about 74 kg m^{-2}, which is high but not unrealistic considering the high SST assumed (30°C).

Figure 12 shows meridional distributions of the zonal flow, potential temperature, water vapor mixing ratio, and the relative humidity. These fields have been averaged zonally and temporally (days 61–80 as in Fig. 11). The thermodynamic fields show that the moisture and temperature profiles are homogeneous over the entire planet, perhaps with the exception of the equatorial plane, which seems slightly colder and drier when compared to the extratropics. The weak meridional temperature gradients are accompanied by weak vertical gradients of the mean zonal flow, which is consistent with the geostrophic balance. In general, the global-scale flow is weak. Meridional distributions of the 20-day-averaged surface precipitation and surface heat fluxes (not shown) demonstrate that the differences between the Tropics and the extratropics are indeed small. The globally averaged surface latent heat flux (about 130 W m^{-2}) balances the globally averaged surface precipitation (about 4.5 mm day^{-1}). The sum of globally averaged surface latent and sensible heat fluxes (about 150 W m^{-2}) balances the prescribed radiative cooling.

The evolution of the mean zonal and meridional flow at the equator is shown in Fig. 13. The mean zonal flow features a descending pattern of westerly winds during the first 60 days, and a predominantly westerly flow across the troposphere in the last 20 days. The descending westerly winds resemble the pattern observed in the two-dimensional cloud-resolving simulations discussed in Held et al. (1993). The mean meridional flow (which represents the globally averaged mass exchange between the Southern and Northern Hemispheres) has pronounced fluctuations with a period of 4–5 days. Wheeler and Kiladis (1999, Fig. 3a) identified similar variability of the meridional flow (the wavenumber zero mixed Rossby–gravity wave with a period of about 4 days) in their analysis of convectively coupled equatorial waves in the terrestrial atmosphere.

Figure 14 shows Hovmöller diagrams of the surface

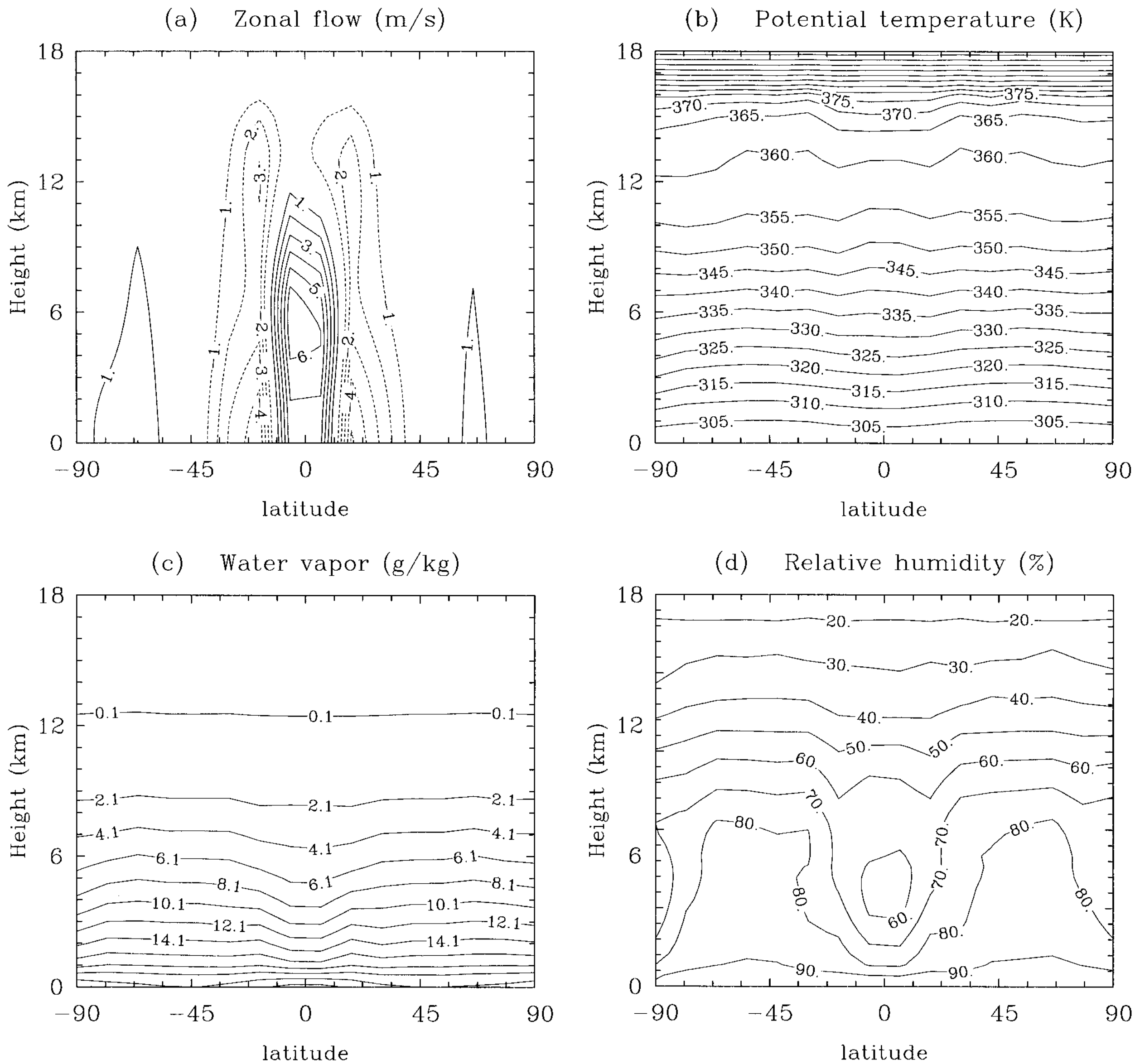

FIG. 12. Meridional distribution of the (a) zonally averaged zonal flow, (b) potential temperature, (c) water vapor mixing ratio, and (d) relative humidity averaged over the last 20 days of the CRCP simulation of the rotating constant-SST aquaplanet.

precipitation in the midlatitudes (about 51°S) and near the equator (for the two rows adjacent to the equator, i.e., for the latitude of about 5.6°S and 5.6°N). These plots are created by combining surface precipitation in 2D CRCP domains at a given latitude, and they illustrate not only the large-scale organization of convection, but propagation of individual cloud systems as well. The midlatitude precipitation does not show any significant large-scale organization of convection. The tropical precipitation, on the other hand, shows a pronounced large-scale organization. In the first half of the simulation, the pattern consists of zonal wavenumber four eastward- and westward-propagating zones of enhanced surface precipitation. The propagation of these zones is shown in Figs. 14b and 14c using lines marked A and B. Propagation speeds are around 3.5 m s^{-1} and around -10 m s^{-1} for A and B, respectively. The eastward-propagating pattern is symmetric with respect to the equator, whereas the westward-propagating pattern is antisymmetric (cf. Figs. 14b and 14c). The strongest surface precipitation is produced at the intersections of the eastward- and westward-propagating patterns. In the second half of the simulation, the surface precipitation near the equator is dominated by an eastward-propagating solitary pattern (along the line marked C, propagation speed of about 8 m s^{-1}). Individual cloud systems inside these zones of enhanced surface precipitation propagate typically from east to west.

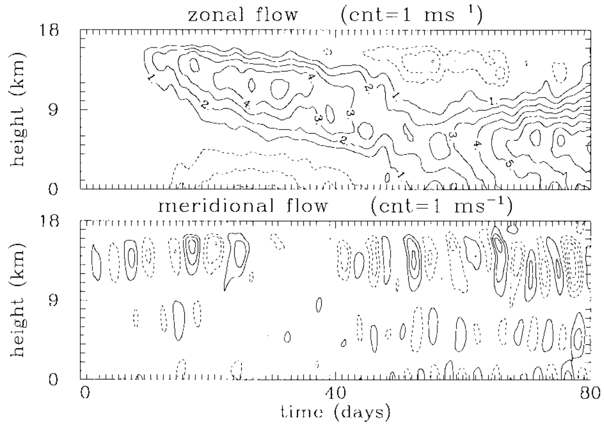

FIG. 13. Time evolution of zonally averaged zonal and meridional velocity components on the equator for the entire 80 days of the CRCP simulation of the rotating constant-SST aquaplanet.

Figures 15 and 16 document the zonal and meridional flow structure associated with the eastward-propagating pattern of enhanced surface precipitation for the period of day 10 to day 30. Figure 15 shows zonal flow perturbation (from the zonal mean), vertical velocity, and the surface precipitation, all at the equator and all averaged in time in the reference frame moving along line A in Figs. 14b and 14c. The figures show that the enhanced surface precipitation is located at the leading edge of the westerly flow perturbations and is associated with large-scale ascending motion (up to about 2 cm s^{-1}) peaking at about 10-km height. Figure 16 shows that the perturbations responsible for large-scale precipitation organization are limited to the equatorial waveguide. The eastward propagation of the perturbations and the fact that the precipitation pattern is centered on the equator suggests that it is associated with the equatorially trapped Kelvin wave, although the meridional flow away from the equator is similar to the equatorially trapped Rossby wave. The propagation speed of the perturbations does not match the speed of convectively coupled Kelvin waves either (e.g., Fig. 3b in Wheeler and Kiladis 1999; Fig. 2b in Wheeler et al. 2000).

Similar analyses for the westward-propagating pattern (line B in Figs. 14b and 14c) are not as definitive as those shown in Figs. 15 and 16. Nevertheless, it appears that the westward-propagating pattern is associated with large-scale flow perturbations having a form of equatorially trapped mixed Rossby–gravity waves, that is, waves with cross-equatorial flow, circulation centered on the equator, and large-scale surface convergence shifted away from the equator. Such flow perturbations are consistent with the surface precipitation pattern shown in Figs. 14b and 14c. However, the propagation speed (about -10 m s^{-1}) does not fit a wavenumber 4 mixed Rossby–gravity wave, which should propagate with a speed of about -20 m s^{-1} (Fig. 3a in Wheeler and Kiladis 1999). Although the large-scale flow does not vanish during the period of this analysis (cf. Fig. 13), its presence is unlikely to explain deviations of the propagation speeds of model-produced perturbations from convectively coupled waves in the equatorial waveguide (Wheeler and Kiladis 1999; Wheeler et al. 2000). The low spatial resolution of the global model might be responsible for such a distorted phase propagation in the CRCP global simulation.

The large-scale organization of convection in the second half of the simulation into a solitary feature is illustrated in Fig. 17. The figure shows snapshots of the surface precipitation pattern together with the surface E–W flow and the total surface heat fluxes for day 80. The wavenumber one surface precipitation pattern in the second half of the simulation (Figs. 14b and 14c) is associated with a coherent structure of surface precipitation, winds, and heat fluxes, which slowly travels from west to east. Except for the solitary structure and its overall strength, the flow and precipitation patterns are similar to the wavenumber four eastward-propagating perturbations observed in the first half of the simulation. For instance, the strong surface precipitation in the equatorial plane occurs on the leading edge of strong surface westerly winds (up to 35 m s^{-1}). The area of enhanced convection and strong westerly winds is associated with large surface heat fluxes (about twice as large as the global mean). Such a pattern of convection, surface flow, and surface heat fluxes is reminiscent of the MJO and an associated westerly wind burst (e.g., Fig. 13 in Lau et al. 1989). The propagation speed of the solitary feature, which travels around the globe in about 60 days (Fig. 14b), fits the observed propagation speed of the MJO.

5. Discussion

The last two sections illustrated the application of the CRCP technique in coupling cloud processes with the large-scale atmospheric dynamics. However, to view the CRCP technique only as a sophisticated subgrid-scale model would not be appropriate. This is because most of the computational cost of the coupled system is associated with running CRCP models; only a small fraction of computations is devoted to the large-scale dynamics. Perhaps a better description is that CRCP involves hundreds or thousands of 2D cloud-resolving models, which communicate with their neighbors in a manner consistent with the large-scale dynamics. Consequently, evolution of the 2D cloud-scale fields within each CRCP domain is directly coupled to the large-scale flow. However, separation of scales becomes a central issue as illustrated by the two-dimensional model results discussed in section 3.

CRCP allows the coupling of not only thermodynamic fields (as classical convection parameterization schemes do), but also momentum fields. Unfortunately, application of the 2D cloud model offers an incomplete picture of the large-scale and cloud-scale momentum

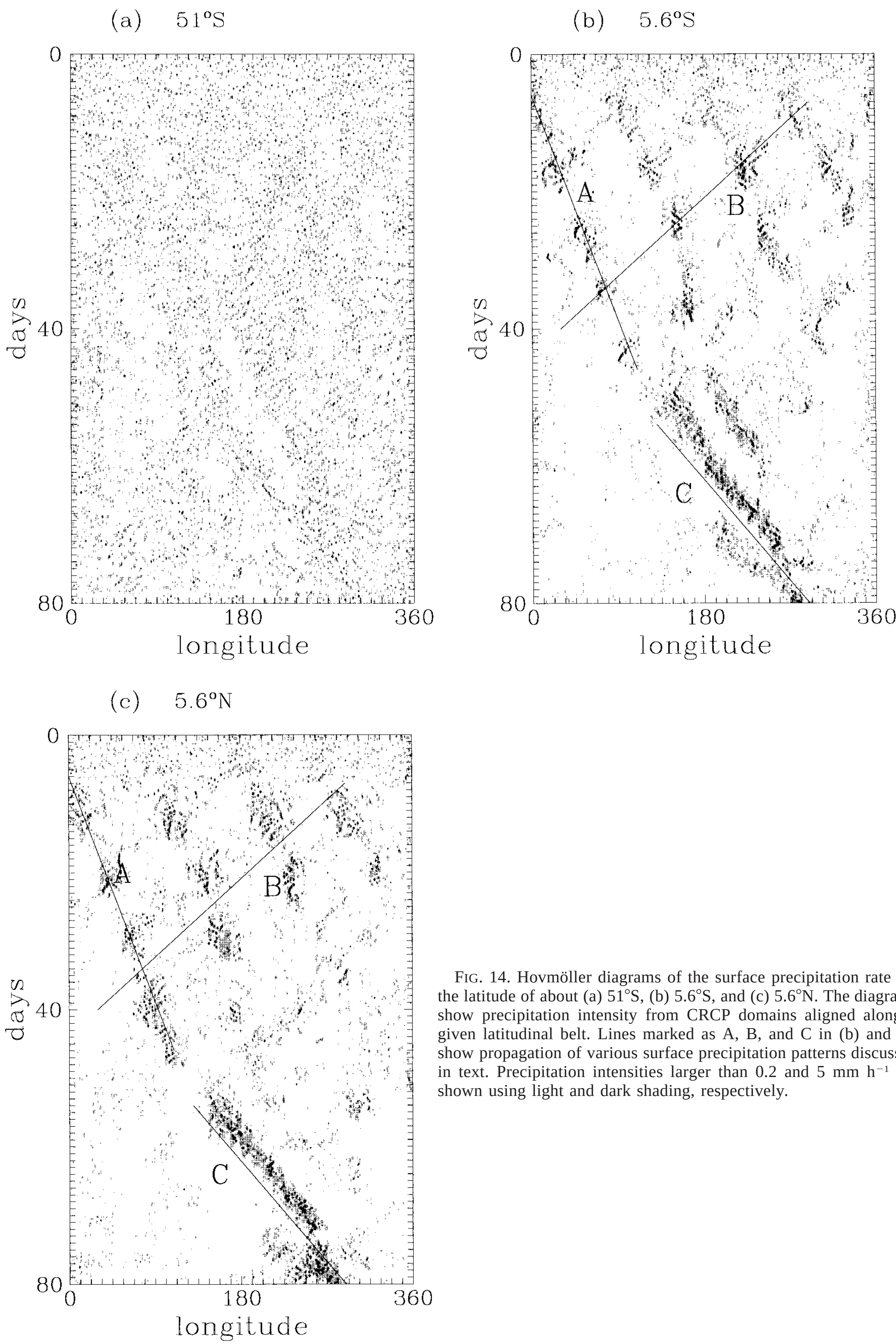

FIG. 14. Hovmöller diagrams of the surface precipitation rate for the latitude of about (a) 51°S, (b) 5.6°S, and (c) 5.6°N. The diagrams show precipitation intensity from CRCP domains aligned along a given latitudinal belt. Lines marked as A, B, and C in (b) and (c) show propagation of various surface precipitation patterns discussed in text. Precipitation intensities larger than 0.2 and 5 mm h^{-1} are shown using light and dark shading, respectively.

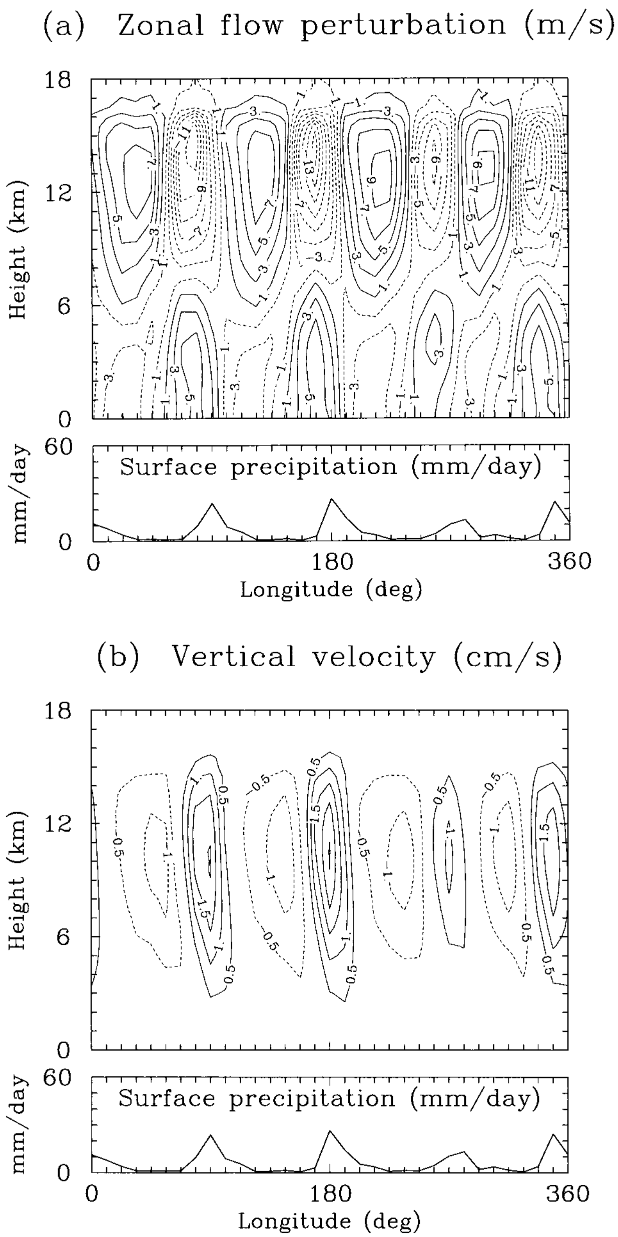

FIG. 15. Perturbations (from the zonal average) of (a) the zonal flow and (b) vertical velocity in the longitude–height plane at the equator. The velocities are sampled in the reference frame moving along the line A in Fig. 14b. Bottom panels show the corresponding distribution of surface precipitation. Solid and dashed contours are for positive and negative values, respectively, and the contour interval is 2 m s^{-1} (0.5 cm s^{-1}) for the horizontal (vertical) velocity.

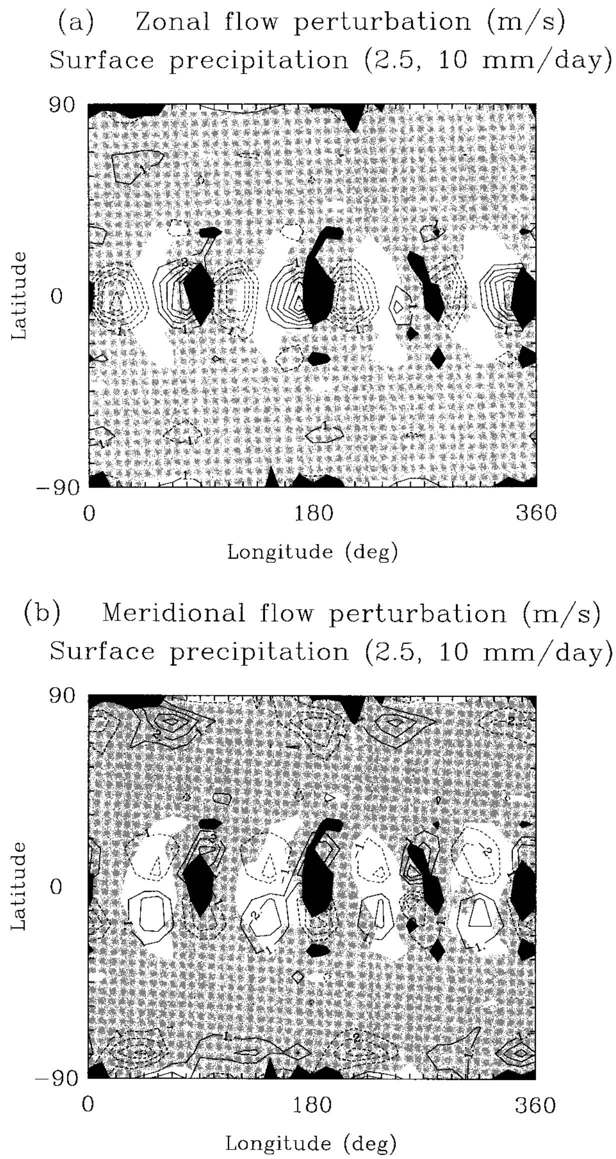

FIG. 16. Perturbations of the (a) zonal and (b) meridional velocities (from the zonal average, solid and dashed contours, contour interval of 1 m s^{-1}), and the surface precipitation distribution (grayscale; light gray represents surface precipitation rate between 2.5 and 10 mm day^{-1}, dark shading represents higher than 10 mm day^{-1}). The data has been averaged as in Fig. 15, i.e., along line A in Fig. 14b.

coupling at best. In the global model application, CRCP domains were aligned in the E–W direction, a strategy motivated by previous cloud-resolving simulations of tropical convection. Lemone and Moncrieff (1994) showed that a 2D framework does offer meaningful results as far as the impact of organized convection on the large-scale momentum field is concerned. This issue can be resolved in the future by applying 3D domains in the CRCP approach. In such a case, both E–W and N–S cloud-scale and large-scale momenta can be coupled simultaneously. Unfortunately, such an approach is beyond the reach of our current computational capabilities unless extremely small 3D domains are applied. Also, CRCP with 3D cloud model domains would offer only minor computational advantages when compared with a fully cloud-resolving large-scale model.

Although computationally intensive even with 2D domains, CRCP is ideal for parallel computations because models from neighboring large-scale columns do not

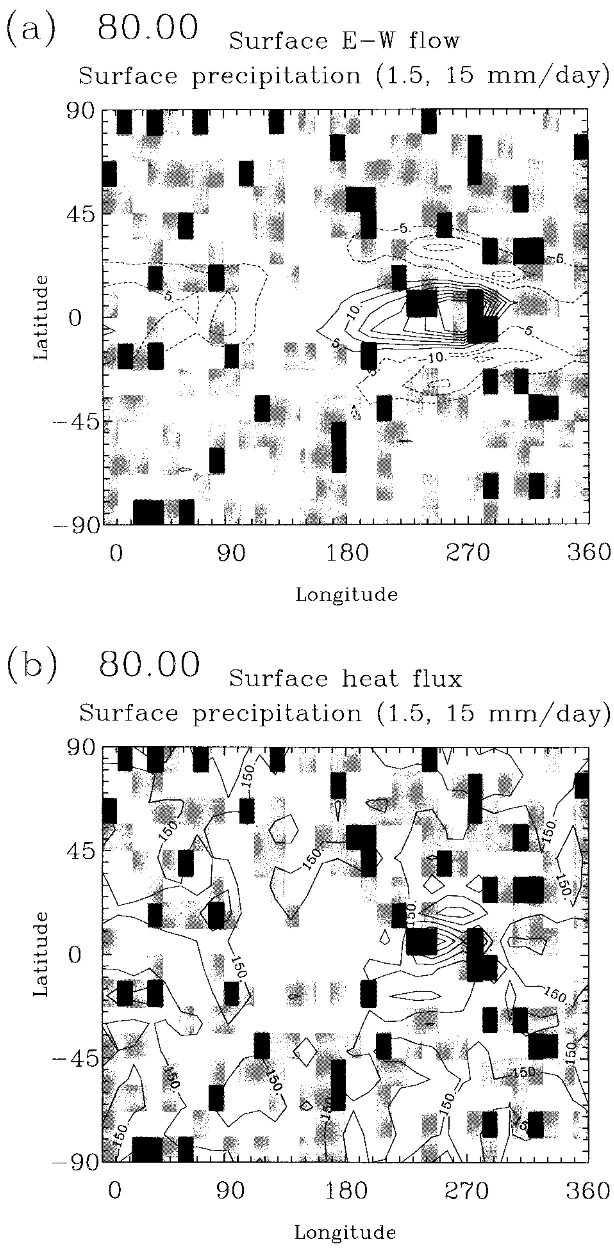

FIG. 17. Snapshot of the surface zonal velocity [(a) solid and dashed contours for positive and negative values, respectively, contour interval of 5 m s^{-1}] and the total surface heat flux [(b) contour interval of 100 W m^{-2} centered at 150 W m^{-2}] at day 80. Grayscale shows surface precipitation rate with precipitation intensity larger than 1.5 and 15 mm h^{-1} is shown using light and dark shading, respectively.

interact with each other during the resolved convection calculation. Consequently, parallel implementation of the large-scale model using CRCP is straightforward: each CRCP model is sent to a different processor and CRCP calculations are done in parallel. It follows that almost perfect scaling occurs with respect to the number of processors used in parallel computations. Such scaling extends up to the point when the number of processors equals the number of columns in the large-scale model. In contrast, classical approaches for parallel computations used in fluid dynamics codes designed for atmospheric applications [such as domain decomposition in the horizontal plane, e.g., Anderson et al. (1997)] scale only when the number of model columns is much larger than the number of processors.

The convective–radiative equilibrium of a 2D nonrotating atmosphere in the presence of SST gradients illustrated the role of scale separation in the CRCP technique (and, consequently, in any convection parameterization scheme as well). Large CRCP domains (e.g., P500) allow the representation of convection organization into mesoscale convective systems within a single CRCP domain. Such domains are typically applied in cloud-resolving simulations of tropical convection driven by large-scale conditions (e.g., Grabowski et al. 1996, 1998, 1999; Wu et al. 1998, 1999). Small CRCP domains (e.g., P20), on the other hand, correspond to the application of convection parameterization in a regional model (e.g., a LAM) with a horizontal grid spacing of a few tens of kilometers. For instance, organization of midlatitude convection into mesoscale convective systems can be simulated with such models (e.g., Zhang et al. 1989, among many others). The expectation is that although convective dynamics has to be parameterized, the mesoscale processes responsible for convection organization can be resolved. This line of thought is also supported by numerical simulation of TOGA COARE and GATE convection using both cloud-resolving (explicit) and parameterized approaches discussed in Su et al. (1999) and in Liu et al. (2001). From this perspective, the failure of the CRCP technique to represent convection organization in the case of the P20 simulations (Fig. 8) might be considered surprising. However, one has to keep in mind that the simulations discussed in Su et al. and in Liu et al. applied strong large-scale forcing, which played an essential role in convective development. When the CRCP technique was applied to the 7-day period of GATE convection [as discussed in Grabowski et al. (1996, 1998) and in Liu et al. (2001)] using CRCP domains of 20–40 km in the horizontal direction, convection organization was successfully simulated in both two (not shown) and three spatial dimensions (Fig. 3 in GS99). Consequently, the ability of a regional model with convection parameterization to represent the development of mesoscale convective systems might depend on the imposed large-scale conditions, such as the strength of the large-scale forcing or the magnitude of the large-scale shear.

The results presented in section 4 (the constant-SST aquaplanet) are very encouraging. However, it is beyond the scope of this paper to put the global CRCP model results properly into the context of the other studies. As far as idealized modeling of the MJO is concerned (or, more generally, modeling of the tropical intraseasonal variability), one should mention the simple beta-plane model of Yano et al. (1995) and at least several aquaplanet studies applying traditional AGCMs with various convection parameterization schemes (the most recent by Chao and Deng 1998; see the review therein and also in Yano et al. 1995). The striking feature of these modeling studies is a sensitivity of model results to the convection parameterization scheme (e.g., Yano et al. 1995; Chao and Deng 1998; see also Slingo et al. 1994).

Much work remains to show that the CRCP approach is superior to traditional approaches in terms of the role of cloud processes in climate. It is not obvious, for instance, how CRCP will perform in the case of warm season midlatitude convection over land for which both Earth rotation and land surface processes are important. Inclusion of a land surface scheme into the CRCP framework to account for more complicated boundary layer processes over land seems straightforward. However, it is uncertain if the 2D framework is sufficient to capture organization of convection in the presence of rotation. One can heuristically defend the CRCP approach in terms of midlatitude convection by pointing out that classical convection parameterization schemes also do not distinguish between deep convection in the Tropics and in midlatitudes. Another issue is the CRCP representation of stratocumulus and shallow convection in subtropics.

The CRCP approach is a novel way to include elements of cloud-scale dynamics into the models of large-scale and global atmospheric flows. This aspect is essential as far as interaction of tropical convection with radiative and surface processes is concerned. As argued in Grabowski (2000), the role of cloud processes (cloud microphysics and dynamics) in the tropical large-scale circulations and climate should be addressed within a framework that resolves cloud dynamics. This is because of complex interactions and feedbacks between small-scale and mesoscale processes (such as cloud dynamics, cloud microphysics, boundary layer and surface processes, and radiative transfer), which are difficult to include using traditional parameterizations. The CRCP technique allows for such interactions in a natural way, albeit in the context of two-dimensional dynamics.

6. Conclusions

This paper tests a novel computational approach, referred to as the Cloud-Resolving Convection Parameterization (CRCP; Grabowski and Smolarkiewicz 1999), designed to couple cloud-scale processes associated with moist atmospheric convection with the large-scale dynamics. The strategy is to use a two-dimensional cloud-resolving model in each column of the large-scale model, an approach motivated by cloud-resolving simulations of tropical convection in two and three spatial dimensions (e.g., Grabowski et al. 1996, 1998, 1999; Wu et al. 1998, 1999). These suggest that a two-dimensional model aligned along the E–W direction with a periodic horizontal domain can capture the gross features of tropical convection and its impact on radiative and surface processes. In the CRCP modeling system, the large-scale model provides forcing for the 2D cloud-scale models in each large-scale model column, and the 2D cloud-scale models feed back the convective response into the large-scale model. This is consistent with classical convection parameterizations. In addition, a simple approach is applied to include E–W momentum coupling between large-scale and cloud-scale models. This aspect is in contrast to classical convection parameterizations, which seldom consider convective momentum transport.

The idealized problem of convective–radiative equilibrium of a 2D nonrotating atmosphere in the presence of SST gradients was used in section 3 to compare CRCP simulations using different horizontal resolutions of the large-scale model (and different sizes of the CRCP domains) against their cloud-resolving counterpart. These simulations illustrate the limitations of CRCP (and convection parameterization in general) associated with the scale separation assumption. CRCP simulations were able to represent large-scale flow reasonably well, but the organization of convection differed among the CRCP simulations and it was different from the cloud-resolving simulation. It can be argued that the generic reason for these results is the inability of small-scale and mesoscale features (such as cold pools or gravity waves) to propagate coherently from one large-scale model column to another. Instead, these features are trapped inside periodic CRCP domains. These features are essential for convection organization (e.g., Moncrieff and Miller 1976; Rotunno et al. 1988; Mapes 1993; Oouchi 1999; Tompkins 2001). When CRCP domains are large enough (say, several hundred kilometers), convection organization is possible within a single CRCP domain, as in the cloud-resolving simulations driven by observed large-scale conditions (e.g., Grabowski et al. 1996, 1998, 1999; Wu et al. 1998, 1999). In this case, however, the large-scale model has low horizontal resolution.

The constant-SST aquaplanet considered in section 4, motivated by a study of Sumi (1992), simulates spontaneous formation of a solitary MJO-type feature propagating west-to-east within the equatorial waveguide with a speed of about 8 m s^{-1} (i.e., circulating the planet in about 60 days). Understanding the physical mechanisms behind the MJO formation, maintenance, and propagation has challenged tropical meteorology since detection of the MJO in the early seventies (see Madden and Julian 1994 and references therein). It is not clear what physical processes are responsible for such a robust MJO simulation considering the very low spatial resolution of the global model. This issue is currently being investigated. However, it should be mentioned that at least some of the mechanisms postulated previously (such as meridional or zonal SST gradients, surface friction, interaction between clouds and radiation, atmosphere–ocean coupling) are de-emphasized based on the physical setup of the CRCP aquaplanet simulation.

It is apparent that CRCP requires more studies to demonstrate its usefulness in addressing the role of cloud processes (deep convection in particular) in large-scale atmospheric dynamics. This is especially important if one considers the high computational cost of the CRCP approach in comparison with traditional convection parameterizations. We anticipate, however, that CRCP will prove to be a valuable tool in the study of cloud and related small-scale and mesoscale processes in the context of large-scale and global atmospheric flows, before cloud-resolving simulations of these flows can be afforded.

Acknowledgments. Numerical experiments were performed using NCAR's HP Exemplar (Scientific Computing Division) and Compaq 8-node AlphaServer 4100 (Mesoscale and Microscale Meteorology Division) parallel computers. The MMM's Compaq cluster was made available through the CiNA Project. Jun-Ichi Yano performed the normal mode analysis presented in section 3. Mirek Andrejczuk's assistance with the incorporation of the CRCP approach into the global model framework is acknowledged. Comments on the manuscript by Brian Mapes, Mitch Moncrieff, Adrian Tompkins, and Jun-Ichi Yano are also acknowledged, as is the editing of the manuscript by James Pasquotto. This work is supported by NCAR's Clouds in Climate Program (CCP).

REFERENCES

Anderson, W. D., V. Grubišić, and P. K. Smolarkiewicz, 1997: Performance of a massively parallel 3D non-hydrostatic atmospheric fluid model. *Proc. Int. Conf. on Parallel and Distributed Processing Techniques and Applications PDPTA '97,* Las Vegas, NV, CSREA, 645–651. [Available from Dr. P. K. Smolarkiewicz, NCAR, P.O. Box 3000, Boulder, CO 80307.]

Chao, W. C., and L. Deng:, 1998: Tropical intraseasonal oscillation, super cloud clusters, and cumulus convection schemes. Part II: 3D aquaplanet simulations. *J. Atmos. Sci.,* **55,** 690–709.

Eisenstat, S. C., H. C. Elman, and M. H. Schultz, 1983: Variational iterative methods for nonsymmetric systems of linear equations. *SIAM J. Numer. Anal.,* **20,** 345–357.

Grabowski, W. W., 1998: Toward cloud resolving modeling of large-scale tropical circulations: A simple cloud microphysics parameterization. *J. Atmos. Sci.,* **55,** 3283–3298.

——, 2000: Cloud microphysics and the tropical climate: Cloud-resolving model perspective. *J. Climate,* **13,** 2306–2322.

——, and P. K. Smolarkiewicz, 1999: CRCP: A cloud resolving convection parameterization for modeling the tropical convecting atmosphere. *Physica D,* **133,** 171–178.

——, X. Wu, and M. W. Moncrieff, 1996: Cloud resolving modeling of tropical cloud systems during Phase III of GATE. Part I: Two-dimensional experiments. *J. Atmos. Sci.,* **53,** 3684–3709.

——, ——, ——, and W. D. Hall, 1998: Cloud resolving modeling of tropical cloud systems during Phase III of GATE. Part II: Effects of resolution and the third spatial dimension. *J. Atmos. Sci.,* **55,** 3264–3282.

——, ——, and ——, 1999: Cloud resolving modeling of tropical cloud systems during Phase III of GATE. Part III: Effects of microphysical parameterizations. *J. Atmos. Sci.,* **56,** 2384–2402.

——, J.-I. Yano, and M. W. Moncrieff, 2000: Cloud-resolving modeling of tropical circulations driven by large-scale SST gradients. *J. Atmos. Sci.,* **57,** 2022–2039.

Held, I. M., R. S. Hemler, and V. Ramaswamy, 1993: Radiative–convective equilibrium with explicit two-dimensional moist convection. *J. Atmos. Sci.,* **50,** 3909–3927.

Kerstein, A. R., 1988: A linear-eddy model of turbulent scalar transport and mixing. *Combust. Sci. Technol.,* **60,** 391–421.

Krueger, S. K., 1993: Linear eddy modeling of entrainment and mixing in stratus clouds. *J. Atmos. Sci.,* **50,** 391–421.

——, and S. M. Lazarus, 1999: Intercomparison of multi-day simulations of convection during TOGA COARE with several cloud resolving and single-column models. Preprints, *23d Conf. on Hurricanes and Tropical Meteorology,* Dallas, TX, Amer. Meteor. Soc., 643–647.

——, C.-W. Su, and P. A. McMurthy, 1997: Modeling entrainment and fine-scale mixing in cumulus clouds. *J. Atmos. Sci.,* **54,** 2697–2712.

Lau, K.-M., L. Ping, C. H. Sui, and T. Nakazawa, 1989: Dynamics of super cloud clusters, westerly wind bursts, 30–60 day oscillations and ENSO: A unified view. *J. Meteor. Soc. Japan,* **67,** 205–219.

Lemone, M. A., and M. W. Moncrieff, 1994: Momentum and mass transport by convective bands: Comparisons of highly idealized dynamical models to observations. *J. Atmos. Sci.,* **51,** 281–305.

Liu, C., M. W. Moncrieff, and W. W. Grabowski, 2001: Hierarchical modeling of tropical convective systems using resolved and parameterized approaches. *Quart. J. Roy. Meteor. Soc.,* **127,** 493–515.

Madden, R. A., and P. R. Julian, 1994: Observations of the 40–50-day tropical oscillation—A review. *Mon. Wea. Rev.,* **122,** 814–837.

Mapes, B. E., 1993: Gregarious tropical convection. *J. Atmos. Sci.,* **50,** 2026–2037.

——, 1998: The large-scale part of tropical mesoscale convective system circulations: A linear vertical spectral band model. *J. Meteor. Soc. Japan,* **76,** 29–55.

Margolin, L. G., P. K. Smolarkiewicz, and Z. Sorbjan, 1999: Large-eddy simulations of convective boundary layers using nonoscillatory differencing. *Physica D,* **133,** 390–397.

Menon, S., P. A. McMurtry, and A. R. Kerstein, 1993: A linear-eddy mixing model for large eddy simulation of turbulent combustion. *Large Eddy Simulation of Complex Engineering and Geophysical Flows,* B. Galperin and S. A. Orszag, Eds., Cambridge University Press, 287–314.

Moncrieff, M. W., and M. J. Miller, 1976: The dynamics and simulation of tropical cumulonimbus and squall line. *Quart. J. Roy. Meteor. Soc.,* **102,** 373–394.

Oouchi, K., 1999: Hierarchical organization of super cloud cluster caused by WISHE, convectively induced gravity waves and cold pool. *J. Meteor. Soc. Japan,* **77,** 907–927.

Raymond, D. J., 1994: Convective processes and tropical atmospheric circulations. *Quart. J. Roy. Meteor. Soc.,* **120,** 1431–1454.

Rotunno, R., J. B. Klemp, and M. L. Weisman, 1988: A theory for strong long-lived squall lines. *J. Atmos. Sci.,* **45,** 463–485.

Slingo, J., and Coauthors, 1994: Mean climate and transience in the Tropics of the UGAMP GCM: Sensitivity to convective parameterization. *Quart. J. Roy. Meteor. Soc.,* **120,** 881–922.

Smolarkiewicz, P. K., and L. G. Margolin, 1994: Variational solver for elliptic problems in atmospheric flows. *Appl. Math. Comput. Sci.,* **4,** 527–551.

——, and ——, 1997: On forward-in-time differencing for fluids: An Eulerian/semi-Lagrangian nonhydrostatic model for stratified flows. *Atmos.–Ocean Special,* **35,** 127–152.

——, and ——, 1998: MPDATA: A finite-difference solver for geophysical flows. *J. Comput. Phys.,* **140,** 459–480.

——, ——, and A. Wyszogrodzki, 2001: A class of nonhydrostatic global models. *J. Atmos. Sci.,* **58,** 349–364.

Soong S.-T., and Y. Ogura, 1980: Response of tradewind cumuli to large-scale processes. *J. Atmos. Sci.,* **37,** 2035–2050.

Su, C.-W., S. K. Krueger, P. A. McMurthy, and P. H. Austin, 1998: Linear eddy modeling of droplet spectral evolution during entrainment and mixing in cumulus clouds. *Atmos. Res.,* **47–48,** 41–58.

Su, H., S. S. Chen, and C. Bretherton, 1999: Three-dimensional week-long simulations of TOGA COARE convective systems using MM5 mesoscale model. *J. Atmos. Sci.,* **56,** 2326–2344.

Sumi, A., 1992: Pattern formation of convective activity over the aqua-planet with globally uniform sea surface temperature (SST). *J. Meteor. Soc. Japan,* **70,** 855–876.

Tompkins, A., 2001: Organization of tropical convection in low vertical wind shears: The role of water vapor. *J. Atmos. Sci.* **58,** 529–545.

Weisman, M. L., W. C. Skamarock, and J. B. Klemp, 1997: The resolution dependence of explicitly modeled convective systems. *Mon. Wea. Rev.,* **125,** 527–548.

Wheeler, M., and G. N. Kiladis, 1999: Convectively coupled equatorial waves: Analysis of clouds and temperature in the wavenumber–frequency domain. *J. Atmos. Sci.,* **56,** 374–399.

——, ——, and P. J. Webster, 2000: Large-scale dynamical fields associated with convectively coupled equatorial waves. *J. Atmos. Sci.,* **57,** 613–640.

Wu, X., W. W. Grabowski, and M. W. Moncrieff, 1998: Long-term behavior of cloud systems in TOGA COARE and their interactions with radiative and surface processes. Part I: Two-dimensional modeling study. *J. Atmos. Sci.,* **55,** 2693–2714.

——, W. D. Hall, W. W. Grabowski, M. W. Moncrieff, W. D. Collins, and J. T. Kiehl, 1999: Long-term behavior of cloud systems in TOGA COARE and their interactions with radiative and surface processes. Part II: Effects of cloud microphysics on cloud–radiation interaction. *J. Atmos. Sci.,* **56,** 3177–3195.

Xu, K.-M., and D. A. Randall, 1996: Explicit simulation of cumulus ensembles with the GATE Phase III data: Comparison with observations. *J. Atmos. Sci.,* **53,** 3709–3736.

Yano, J. I., J. C. McWilliams, M. W. Moncrieff, and K. A. Emanuel, 1995: Hierarchical tropical cloud systems in an analog shallow-water model. *J. Atmos. Sci.,* **52,** 1723–1741.

Zhang, D.-L., K. Gao, and D. B. Parsons, 1989: Numerical simulation of an intense squall line during 10–11 June 1985 PRE-STORM. Part I: Model verification. *Mon. Wea. Rev.,* **117,** 960–994.